Phase-Field Modeling of Interfacial Dynamics in Emulsion Flows: Nonequilibrium Surface Tension

A. Lamorgese* and R. Mauri

Department of Civil and Industrial Engineering,
Laboratory of Multiphase Reactive Flows,
Università di Pisa, I-56126 Pisa, Italy

Abstract

A weakly nonlocal phase-field model is used to define the surface tension in liquid binary mixtures in terms of the composition gradient in the interfacial region so that, at equilibrium, it depends linearly on the characteristic length that defines the interfacial width. Contrary to previous works suggesting that the surface tension in a phase-field model is fixed, we define the surface tension for a curved interface and far-from-equilibrium conditions as the integral of the free energy excess (i.e., above the thermodynamic component of the free energy) across the interface profile in a direction parallel to the composition gradient. Consequently, the nonequilibrium surface tension can be widely different from its equilibrium value under dynamic conditions, while it reduces to its thermodynamic value for a flat interface at local equilibrium. In nonequilibrium conditions, the surface tension changes with time: during mixing, it decreases as the inverse square root of time, while in the linear regime of spinodal decomposition, it increases exponentially to its equilibrium value, as nonlinear effects saturate the exponential growth. In addition, since temperature gradients modify the steepness of the concentration profile in the interfacial region, they induce gradients in the nonequilibrium surface tension, leading to the Marangoni thermocapillary migration of an isolated drop. Similarly, Marangoni stresses are

*Email: andrea.lamorgese@unipi.it.

induced in a composition gradient, leading to diffusiophoresis. We also review results on the nonequilibrium surface tension for a wall-bound pendant drop near detachment, which help to explain a discrepancy between our numerically determined static contact angle dependence of the critical Bond number and its sharp-interface counterpart from a static stability analysis of equilibrium shapes after numerical integration of the Young-Laplace equation. Finally, we present new results from phase-field simulations of the motion of an isolated droplet down an incline in gravity, showing that dynamic contact angle hysteresis can be explained in terms of the nonequilibrium surface tension.

1. Introduction

In a liquid-vapor system at equilibrium, a molecule in the liquid bulk is surrounded by attractive neighbors, while a molecule at the surface, being attracted by a reduced number of molecules, finds itself in an energetically unfavorable state (see de Gennes et al., 2004). The resulting free energy deficit (i.e., a negative surplus) per unit interfacial area is a thermodynamic equilibrium property of the interface and can be identified macroscopically as the surface tension.

This microscopic picture is reflected at the mesoscale in the phase-field model, an approach that goes back to van der Waals (1894) and has been widely used to describe many equilibrium interfacial properties. Here, on one hand, the continuum hypothesis is assumed to be valid, so that thermodynamic quantities such as temperature and pressure can be defined locally, even when, as it usually occurs in continuum mechanics, they are not uniform in space. In addition, weakly nonlocal effects are taken into consideration, so that thermodynamic potentials depend on the gradients of the order parameter, i.e., density or concentration. Accordingly, an interface is described as a finite thickness transition region where the order parameter is allowed to change continuously, interpolating between the two phases. Naturally, as the surplus interfacial energy is defined in terms of density (or concentration) gradients, it is natural to generalize the concept of surface tension to systems far from equilibrium (see

the discussion in Joseph and Renardy, 1993).

Many authors have studied nonequilibrium micro- and meso-scale interpretations of the surface tension. For example, Ma et al. (1992) confirmed the microscopic nature of surface tension by numerically simulating a binary system at equilibrium using molecular dynamics. At the mesoscale, several coarse-grained expressions for the free energy can be found in the literature (see Hohenberg and Halperin, 1977), which have allowed to model dynamical processes such as mixing and demixing. Since the surplus free energy depends on the density (or concentration) gradients in the interfacial region, a nonequilibrium surface tension can be defined, which characterizes the system during the whole process. This, in turn, can be considered as the appropriate jump boundary condition of any macroscopic multiphase flow model, where interfaces are considered to be zero-thickness surfaces (see Sagis, 2011). Applications of the phase-field model to dynamic processes in fluids lead to the introduction into the Navier-Stokes equation of a nonequilibrium capillary force, generally referred to as the Korteweg force. As it arises naturally by applying Hamilton's least action principle, this is a reversible body force, tending to restore the local equilibrium condition (Lamorgese et al., 2011). As such, the Korteweg force tends to accelerate both the mixing process of miscible fluids and the phase separation of unstable or metastable mixtures.

The remainder of this paper is laid out as follows. In Sect. 2 we review the formulation of a diffuse-interface model of inhomogeneous binary fluids [a.k.a. square-gradient theory or Model H, in the taxonomy of Hohenberg and Halperin (1977)], based on a regular solution model along with a Flory-Huggins and Cahn-Hilliard type of modeling for the excess (i.e., enthalpic) and nonlocal components of the Gibbs free energy of mixing. We then show the definition of the surface tension for a flat interface at local equilibrium and briefly discuss its extension to curved interfaces and far-from-equilibrium conditions. Subsequently, we recall the equations governing dynamic processes (under isothermal conditions) before discussing some previously published results from simulations of binary fluid mixing and demixing, and of the Marangoni migration of isolated

drops in a temperature (or concentration) gradient. We also discuss previous results on the nonequilibrium surface tension at pinchoff from simulations of the buoyancy-driven detachment of a wall-bound pendant drop. Finally, we discuss contact angle hysteresis in phase-field simulations of the motion of an isolated drop down an incline in gravity. Conclusions are then presented.

2. Model Description

Consider a regular binary mixture, composed of two incompressible liquids A and B having the same molar density, ρ. The phase-field model can be derived assuming that its free energy is the sum of a thermodynamic part and a nonlocal contribution (see Cahn and Hilliard, 1958, 1959; Lamorgese et al., 2011), i.e.,

$$G = \rho RT \int_V \tilde{g} dV, \qquad \tilde{g}\left(\phi, \nabla\phi\right) = g\left(\phi\right) + \frac{1}{2}a^2\left(\nabla\phi\right)^2, \tag{1}$$

where g is the dimensionless thermodynamic (i.e., coarse-grained) bulk free energy density, T is the temperature and V the volume, R is the gas constant, while a indicates a typical length. Equation (1) can be justified rigorously starting from Landau's mean-field theory for a nonhomogeneous van der Waals fluid (Landau and Lifshitz, 1980), showing that in addition to the above thermodynamic part, spatial inhomogeneities in the composition give rise to a nonlocal (square-gradient) component of the coarse-grained free energy, typical of the diffuse-interface model. That derivation is valid for equilibrium and nonequilibrium conditions alike. At local equilibrium, when the mixture is separated into two phases α and β by a flat interfacial region, a surface tension can be obtained by integrating the specific (i.e., per unit volume) free energy along a coordinate z perpendicular to the interface, i.e.,

$$\sigma = \frac{1}{2}a^2\rho RT \int_{-\infty}^{\infty} \left(\nabla\phi\right)^2 dz, \tag{2}$$

where we have considered that the composition of the mixture far from the interfacial region is constant. This result was first obtained by van der Waals (1894) in his treatment of the equilibrium liquid-vapor interface for a single-component fluid and was applied by Cahn and Hilliard (1959) to a binary mixture (see also

de Gennes, 1985). More recently, Pismen (2001) showed a systematic derivation of the van der Waals square-gradient model based on a mean-field approximation along with a gradient expansion for the order parameter. This derivation was an intermediate result (Pismen and Pomeau, 2000) as they were trying to obtain an expression for the disjoining pressure based on a more accurate free energy functional (with a more realistic representation of nonlocal interactions). On the other hand, Jacqmin (2000) performed a careful matched asymptotic analysis showing that, in the limit of vanishing interfacial width, the diffuse-interface model is consistent with the usual Marangoni-type boundary conditions that arise in the classical formulation of two-phase flow. Note that the asymptotic analysis of diffuse-interface models has been furthered considerably (Magaletti et al., 2013; Sibley et al., 2013a) since the Jacqmin (2000) paper. In particular, recent work by Sibley et al. (2013a) has shown that when a binary fluid diffuse-interface model is employed in conjunction with a tensorial mobility, the model allows the classical two-phase flow equations to be recovered to all orders in the Cahn number, in the limit as it tends to zero.

Considering that the expression for the free energy, Eq. (1), is valid also for systems far from equilibrium, the surface tension as defined in Eq. (2) is not necessarily confined to systems at thermodynamic equilibrium. In fact, a similarly defined nonequilibrium surface tension had already been introduced in Ma et al. (1993), Osborn et al. (1995) and Swift et al. (1996), particularly for checking their lattice Boltzmann scheme in terms of the rate of decay of a flat interface (initially at equilibrium) which is instantaneously brought from the two-phase to the one-phase region. However, these authors did not clarify the role of the nonequilibrium surface tension in diffuse-interface models of emulsion flows far from the critical point, which is the primary objective of the work reported herein.

Again, it should be stressed that Eq. (1) represents a coarse-grained expression of the free energy, so that a is in no way equal to the actual interfacial thickness. Assuming that the mixture has zero excess volume of mixing and zero excess entropy of mixing, the simplest expression for the thermodynamic

free energy density, g, corresponding to a perfectly symmetric, partially miscible binary mixture, is the sum of an entropic, ideal part, and a nonideal, so-called excess part, with

$$g = g_0 + \phi \ln \phi + (1 - \phi) \ln (1 - \phi) + \Psi \phi (1 - \phi) . \tag{3}$$

Here, g_0 is the free energy of both the pure components (they must be equal, since we are considering an ideally perfectly symmetric binary mixture), ϕ is the molar (and mass) concentration of species A, while Ψ is the temperature-dependent Margules parameter (see Sandler, 2006). Since the entropy of mixing for regular mixtures is equal to that for an ideal gas, the excess free energy of mixing cannot depend on temperature and, therefore, Ψ and a^2 must be inversely proportional to T. Thus, considering that at the critical point (see below), when $T = T_c$, $\Psi = \Psi_c = 2$, we may assume:

$$\Psi = \frac{2T_c}{T}, \qquad a = \hat{a}\sqrt{\frac{2T_c}{T}} = \hat{a}\sqrt{\Psi}, \tag{4}$$

where $\hat{a}$ is a constant length, independent of the temperature. Since at constant pressure and temperature $dg = \mu d\phi$, where $\mu = \mu_A - \mu_B$ is the dimensionless chemical potential difference, we obtain:

$$\mu = \frac{dg}{d\phi} = \ln \frac{\phi}{1 - \phi} + \Psi (1 - 2\phi) . \tag{5}$$

Phase separation occurs whenever the temperature of the system T is lower than the critical temperature T_c. Imposing that at the critical point $d^2g/d\phi^2 = 0$ and $\phi = 1/2$, we find that $\Psi_c = 2$ is the critical value of Ψ. Therefore, the single-phase region of the phase diagram corresponds to values $\Psi < 2$, while when $\Psi > 2$ the mixture presents a miscibility gap. In the latter case, there is an interval $\left(\phi_e^\beta, \phi_e^\alpha\right)$ in the mixture composition, such that when $\phi < \phi_e^\beta$ and $\phi > \phi_e^\alpha$ the mixture is single-phase, while when $\phi_e^\beta < \phi < \phi_e^\alpha$ it is segregated into two coexisting phases. In this case, the two phases have compositions ϕ_e^α and ϕ_e^β (here $\phi_e^\beta = 1 - \phi_e^\alpha$ out of symmetry) that can be determined imposing $\mu = 0$ in Eq. (5). For example, a 50% acetone - 50% hexadecane mixture at ordinary conditions of temperature and pressure separates in two phases, with

$(0.3, 0.7)$ and $(0.7, 0.3)$ compositions, so that the mixture is well-described by Eq. (3), with $\Psi = 2.12$, while when the two phases have $(0.1, 0.9)$ and $(0.9, 0.1)$ compositions, we find $\Psi = 2.75$. In particular, near the critical point, denoting

$$u = 2\phi - 1, \qquad \psi = \Psi - 2, \tag{6}$$

with $\psi \ll 1$ and $|u| \ll 1$, we obtain

$$\mu = \frac{2}{3}u^3 - u\psi, \tag{7}$$

so that from $\mu = 0$ we easily find: $u = \pm u_e = \pm\sqrt{3\psi/2}$. Note that $\psi = O\left(u_e^2\right)$, thus confirming that the two terms on the RHS of Eq. (7) have the same magnitude. Now, assuming that the mixture is nonhomogeneous, at equilibrium the total free energy G in Eq. (1) is minimum, subjected to the mass conservation constraint. Accordingly, the thermodynamic condition stating that $\mu = 0$ at equilibrium is generalized to become $\tilde{\mu} = 0$, where:

$$\tilde{\mu} = \frac{\delta\tilde{g}}{\delta\phi} = \frac{\partial\tilde{g}}{\partial\phi} - \nabla\cdot\frac{\partial\tilde{g}}{\partial\nabla\phi} = \mu - a^2\nabla^2\phi. \tag{8}$$

This can be considered as a definition of generalized chemical potential difference, a fundamental element of the phase-field model.

2.1. Thermodynamic limit

As mentioned above, at local equilibrium the generalized chemical potential difference (8) must vanish. Assuming that the mixture has a flat interfacial region centered around the $z = 0$ plane, so that $u = u(z)$, with $u(0) = 0$ and $u(\infty) = u_e$, the condition $\tilde{\mu} = 0$ can be easily integrated to find the concentration profile. In particular, in Fig. 1 we show that the concentration profile far from the critical condition (i.e., for $\Psi = 2.7$ in this case) is well-approximated by the concentration profile near the critical point, i.e., the van der Waals result (van der Waals, 1894):

$$\tilde{\mu} = 0 \quad \rightarrow \quad u(z) = \sqrt{\frac{3}{2}\psi}\tanh\left(\frac{z}{\lambda}\right), \text{ where } \lambda = \frac{a}{\sqrt{\psi}}. \tag{9}$$

Therefore, the surface tension can be determined by applying Eq. (2), finding:

$$\sigma = \frac{\psi^{3/2}}{4}a\rho RT. \tag{10}$$

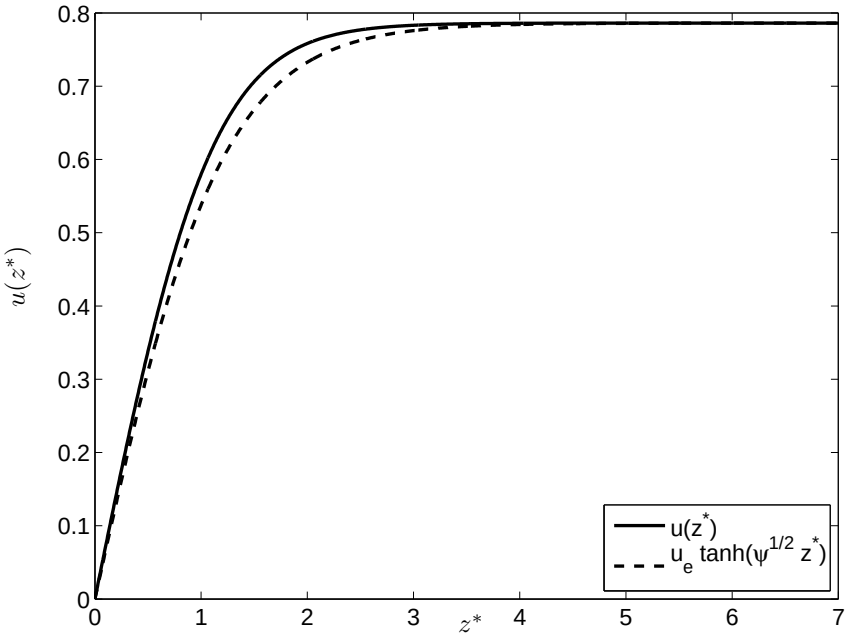

Figure 1: Flat interface concentration profile obtained by shooting on the 1D Cahn-Hilliard equation for $\Psi = 2.7$ (solid) vs. hyperbolic tangent profile $u_0(z^*) = u_e \tanh(\psi^{1/2} z^*)$ with $z^* \equiv z/a$ (dashed).

In general, the surface tension for a flat interface at equilibrium can be written as

$$\sigma = \kappa a \rho RT, \tag{11}$$

where κ is represented in Fig. 2 as a function of ψ. Far from the critical point, as we see that $\kappa = O\left(10^{-1}\right)$, we can evaluate a from the surface tension. In fact, considering that $\rho RT \approx 10^4\,\mathrm{kJ/m^3}$ and $\sigma \approx 10^{-2}\,\mathrm{N/m}$, we obtain: $a \approx 0.01\,\mu\mathrm{m}$, showing that, as expected, a is a mesoscale length and, therefore, it is larger than the microscopic interface thickness. It should be acknowledged that a could also be obtained from a rigorous theoretical expression involving the attractive part of a pairwise intermolecular potential (Henderson, 1995; Pismen, 2001; Molin and Mauri, 2007; Lamorgese et al., 2011; Sibley et al., 2013b); however, in practical applications of square-gradient theory (including the one reported herein) the square-gradient coefficient is adjusted by fitting to experimental

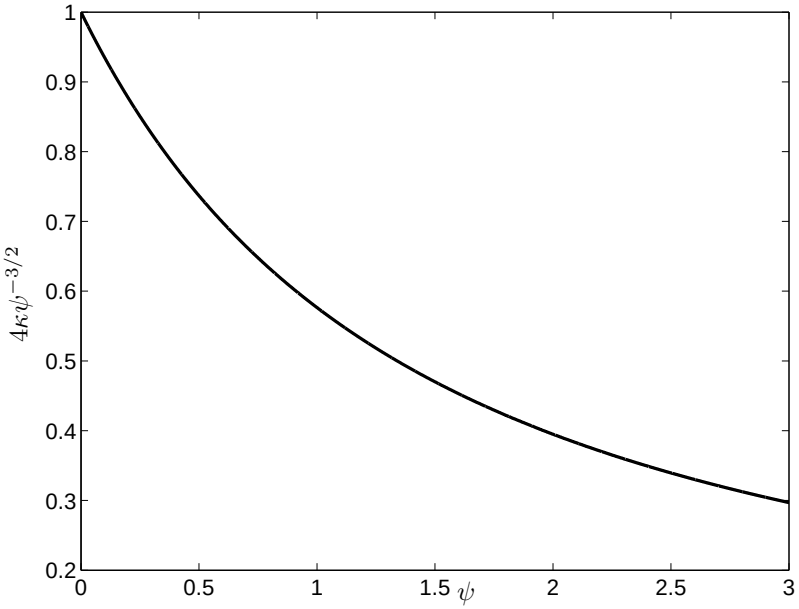

Figure 2: Dimensionless magnitude of the line integral of the square-gradient free energy for a flat interface profile at equilibrium as a function of the Margules parameter.

surface tension data for binary mixtures (e.g., see the discussion in Llovell et al., 2012). In other words, at a given temperature a is computed from Eq. (11) assuming that the (equilibrium) surface tension is known. Incidentally, this allows the nonequilibrium surface tension to reduce to its thermodynamic value for a flat interface at local equilibrium. It would be naive to think that another option is to fix a and calculate the surface tension from Eq. (11) since this would be inconsistent with the gradient expansion employed to arrive at the square-gradient free energy functional. Obviously, a and the equilibrium surface tension cannot be prescribed independently and still be consistent with Eq. (11).

2.2. Dynamic processes

When the system finds itself in a state of nonequilibrium, it evolves following its governing equations, expressing the conservation of mass, chemical species, momentum and energy. Those equations can be derived on the mesoscale using a dissipative minimization procedure (Serrin, 1959) wherein balance equations are

first obtained for a nondissipative fluid as the extremal conditions of an action functional, after which the equations are augmented with terms corresponding to the relevant molecular transport coefficients. In fact, the governing equations can also be obtained from a nonequilibrium statistical mechanical description of the fluid mixture taken as a system of interacting particles, known as dynamical density functional theory (DDFT), which generalizes the classical equilibrium density functional theory (square-gradient theory in our case) towards nonequilibrium situations. While DDFT can be derived from sub-microscopic equations such as the Smoluchowski equation (Archer and Evans, 2004) or the Langevin equations (Marconi and Tarazona, 2000) for individual particles, many approximations are normally involved in the derivations including an adiabatic approximation, as well as a local equilibrium assumption. For an assessment of those approximations, particularly in the context of multispecies colloidal fluid mixtures treated via DDFT, see Goddard et al. (2013) and references therein.

In what follows we assume isothermal conditions and therefore ignore the energy balance equation. [Note, however, that diffuse-interface models for both single-component and binary fluids with the energy equation included have been discussed in the literature many times (Araki and Tanaka, 2004; Onuki and Kanatani, 2005; Onuki, 2007; Lamorgese and Mauri, 2011; Liu et al., 2013; Guo and Lin, 2015).] Therefore, the governing equations are:

$$\rho \frac{D\phi}{Dt} = -\nabla \cdot \mathbf{J}_\phi, \tag{12}$$

$$\nabla \cdot \mathbf{v} = 0, \tag{13}$$

$$\rho \frac{D\mathbf{v}}{Dt} + \nabla p = \eta \nabla^2 \mathbf{v} + \mathbf{F}_\phi, \tag{14}$$

where $\frac{D}{Dt} = \frac{\partial}{\partial t} + \mathbf{v} \cdot \nabla$ is the material derivative, $\mathbf{v}$ is the average local fluid velocity, $\mathbf{J}_\phi$ is the diffusion flux, and $\mathbf{F}_\phi$ is the Korteweg nonequilibrium body force. As shown by Mauri et al. (1996), applying nonequilibrium thermodynamics we see that $\mathbf{J}_\phi$ is proportional to the gradient of the generalized chemical potential difference through the relation

$$\mathbf{J}_\phi = -\rho D \phi (1 - \phi) \nabla \tilde{\mu}, \tag{15}$$

where D is the molecular diffusivity. This constitutive relation reduces to the traditional Fick's law in the dilute limit, i.e., when $\phi \to 0$ or $\phi \to 1$.

The Korteweg body force $\mathbf{F}_\phi$ equals the generalized gradient of the free energy and therefore it is driven by the generalized chemical potential gradients, i.e.,

$$\mathbf{F}_\phi = \rho RT \frac{\delta \tilde{g}}{\delta \mathbf{r}} = \rho RT \tilde{\mu} \nabla \phi = -\rho RT \phi \nabla \tilde{\mu}, \tag{16}$$

where the $\nabla(\phi\tilde{\mu})$ term can be reabsorbed into the pressure gradient in Eq. (14) and therefore does not play any role here, due to the divergence-free condition. [The variety of similar ways to incorporate the Korteweg force has also been addressed in Sibley et al. (2013a).] In particular, when the system presents well-defined sharp phase interfaces, such as at the late stages of phase separation, this body force reduces to the conventional surface tension. Therefore, being proportional to $-\nabla\tilde{\mu}$, which is identically zero at local equilibrium, $\mathbf{F}_\phi$ can be thought of as a reversible nonequilibrium capillary force, tending to restore the local equilibrium condition. Finally, note that, since $\mu\nabla\phi = \nabla g$, the Korteweg force can be expressed in any one of the following forms:

$$\mathbf{F}_\phi = \rho RT a^2 \phi \nabla \nabla^2 \phi = -\rho RT a^2 \nabla\phi \nabla^2 \phi. \tag{17}$$

Comparing Eq. (17) with (11) we see that $F_\phi \approx \sigma/(\kappa a^2)$; in addition, assuming that the inertial forces are negligible compared to their viscous counterparts (i.e., assuming low Reynolds numbers), from Eq. (14) we obtain: $v \approx F_\phi a^2/\eta$, i.e., $v \approx \sigma/(\kappa\eta)$. Therefore, the ratio between convective mass fluxes, $\rho v\phi$, and diffusive fluxes, $J_\phi \approx \rho D/a$ gives the so-called fluidity number (Tanaka and Araki, 1998):

$$\alpha \equiv \frac{\rho RT a^2}{\eta D} = \frac{\sigma a}{\kappa \eta D}. \tag{18}$$

For liquid mixtures, where typically $\eta \approx 10^{-3}\,\mathrm{kg/(m\,s)}$ and $D \approx 10^{-9}\,\mathrm{m^2/s}$, we obtain: $\alpha \approx 10^3$. On the other hand, for alloys and very viscous mixtures $\alpha \ll 1$ and therefore, in the absence of forced convection, the mass transfer process can be considered as purely diffusive.

2.3. Mixing and demixing

Consider a 50% - 50% hexadecane-acetone binary mixture at a temperature of 20°C, where at thermodynamic equilibrium two coexisting phases are present, separated by a thin interface. Now, when the mixture is heated to above its critical temperature, $T_c = 27$°C, it starts to mix, i.e., the interfacial region appears to thicken in time. As shown by Santonicola et al. (2001), this process is very slow, as after one hour the interfacial region is only a few millimeters thick. On the other hand, when the mixture is quenched back to 20°C, the ensuing phase separation process is very rapid and a two-phase equilibrium state is reached within a few seconds (Califano and Mauri, 2004; Califano et al., 2005).

To explain this behavior, let us describe first the mixing process, assuming that the mixture is initially quiescent and phase separated (with $\Psi > 2$) along a flat interface at $z = 0$, and is then instantaneously heated, so that $\Psi < 2$ at all times $t \geq 0$. Then, as shown in Lamorgese and Mauri (2006), when $t \gg a^2/D$ the process is purely diffusive and is well-approximated by the diffusion equation:

$$\frac{\partial \phi}{\partial t} = D^* \frac{\partial^2 \phi}{\partial z^2}, \quad \text{with } D^* = D[1 - 2\Psi\bar{\phi}(1 - \bar{\phi})], \tag{19}$$

where $\bar{\phi}$ represents the mean value of ϕ. Since the results of our simulations are in excellent agreement with the similarity solution resulting from Eq. (19), we may conclude that the mixing process of two fluids separated by an initially flat sharp interface remains one-dimensional, and is a purely diffusive process, with an effective diffusivity D^* that depends on the thermodynamic properties of the mixture, such as the Margules parameter. Therefore, from the surface tension definition, Eq. (2), we easily obtain:

$$\sigma = \frac{a^2 \rho R T}{\sqrt{8\pi}\lambda}, \tag{20}$$

where $\lambda = \sqrt{4D^* t}$ is the thickness of the interfacial region. The same result is obtained whenever the initial configuration is one-dimensional, as in the case of an isolated drop. Thus, in liquid mixtures, as $D \approx 10^{-9}\,\mathrm{m}^2/\mathrm{s}$, we see that

within half an hour we expect the interfacial region to be $O\,(1\,\mathrm{mm})$ thick, in agreement with experimental observations (Santonicola et al., 2001).

Now, let us consider the demixing process of very viscous mixtures with $\alpha \ll 1$, i.e., when convection is negligible, assuming that the mixture is initially well-mixed, and then instantaneously quenched to below the spinodal curve, so that $\Psi > 2$ at $t > 0$. As shown by Cahn and Hilliard (1958, 1959) and Cahn (1961), near the critical point, i.e., when $\psi \ll 1$, this process can be studied using a linear stability analysis. In fact, Eq. (12) reduces to the linearized Kuramoto-Sivashinsky equation

$$\frac{\partial u}{\partial t} = -2\psi\nabla^2 u - \nabla^4 u, \tag{21}$$

where the spatial and time coordinates have been made dimensionless in terms of a and $4a^2/D$, respectively. Assuming a periodic perturbation

$$u = u_0 \exp\left(i\mathbf{k}\cdot\mathbf{r} + t/\tau\right), \tag{22}$$

we see that the initial uniform concentration field is unstable provided that $k < \sqrt{2\psi}$. In particular, the exponential growth τ^{-1} of the disturbance is maximized when $k = \sqrt{\psi}$, which corresponds to a characteristic time $\tau = 4a^2/(D\psi^2)$. Correspondingly, the nonequilibrium surface tension increases exponentially to its equilibrium value, as nonlinear effects saturate the exponential growth. At the end [i.e., for $t \simeq O(\tau)$], the system consists of well-defined single-phase microdomains [whose typical size is still $O(a)$] in which the average concentration is not too far from its equilibrium value (though the system is still far from local equilibrium). At this point, in cases where diffusion is the only relevant transport mechanism (as with polymer melts and alloys), nuclei grow slowly (Lifshitz and Slyozov, 1961) with time, like $R \sim t^{1/3}$, with R denoting the characteristic nucleus size. On the other hand, when the mixture is a low viscosity liquid, at end of the linear regime the mechanism of growth is convection-driven coalescence, which implies that drops move against each other under the action of an attractive, nonequilibrium capillary (a.k.a. the Korteweg) force. In fact, considering that the Korteweg force balances the viscous forces, as shown in

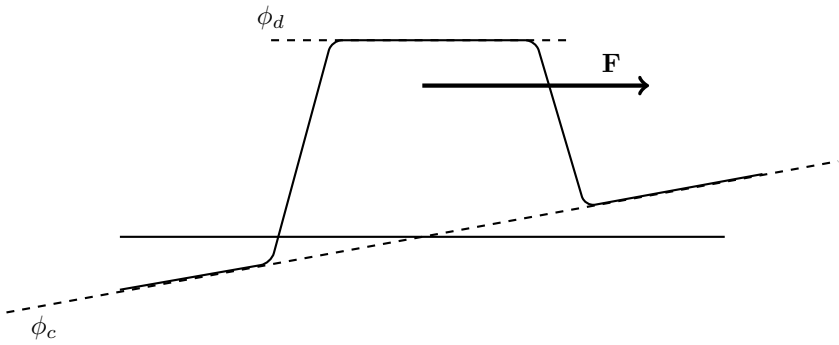

Figure 3: Schematic of isolated drop with mass fraction $\phi_d = 1 - \phi_c$ embedded in a continuous phase having an initial concentration gradient $\nabla\phi_c$.

Vladimirova et al. (1999b), we find that nuclei grow linearly with time, with a constant growth rate which, for the previously noted acetone-hexadecane system, turns out to be $dR/dt \approx 100\,\mu$m/s, in agreement with experimental observations (Gupta et al., 1999). Then, as soon as the nuclei reach a limit size of about 1 mm, which is approximately one-tenth the capillary length in the experiments by Califano and Mauri (2004), they rapidly sediment, leading to an equilibrium state with two coexisting phases, within a time of about 10 s, in agreement with experimental observations (Califano and Mauri, 2004; Califano et al., 2005).

2.4. Marangoni effects

Marangoni effects consist of all types of convection resulting from interfacial tension gradients. Two important examples of Marangoni effects are the movement of a single spherical drop of radius R, induced by surface tension gradients due to variations of temperature or of composition. In the first case, which is generally referred to as thermocapillary migration, since surface tension is (in general) a decreasing function of temperature, it will be larger on the cold side of the drop, thus inducing a Marangoni force per unit area $(-\nabla\sigma)$ (from larger to small surface tension) acting upon the drop. Assuming that, at low Reynolds number, this capillary stress balances the viscous stress, $\eta|\mathbf{V}|/R$, where $\mathbf{V}$ is

the drop velocity, we obtain:

$$\mathbf{V} = C\frac{R}{\eta}(-\nabla\sigma), \tag{23}$$

where C is an $O(1)$ constant. This problem was solved exactly by Young et al. (1959) who, in particular, found that when both the viscosity and thermal conductivity of the drop are, respectively, equal to those for the continuous phase, then $C = 2/15$. Within the phase-field framework, we observe from Eq. (4) that the warmer side of the interfacial region of the drop has a smaller interfacial thickness a, and therefore it will present a larger concentration gradient and a smaller surface tension, compared to the colder region. Therefore, from Eq. (23) we have:

$$\mathbf{V} = C\kappa\frac{\alpha RD}{\hat{a}}(-\nabla\Psi), \tag{24}$$

where we have substituted from Eq. (18) and based on Eq. (4) we have considered that $\nabla a^{-1} \propto \nabla\Psi/\hat{a}$. This expression is in good agreement with the explicit result obtained in 2D by Lamorgese and Mauri (2011) who found $\mathbf{V} = 0.029\frac{\alpha RD}{\hat{a}}(-\nabla\Psi)$. This situation corresponds to the quasi-static motion of a near-local-equilibrium droplet when the Marangoni (and Reynolds) number is very small, so that the drop moves with a constant velocity which is in good agreement with the Marangoni velocity. Roughly speaking, the drop goes through a sequence of quasi-equilibrium states, each one having an (equilibrium) surface tension corresponding to its thermodynamic value at that particular temperature. This is in contrast with the far-from-equilibrium conditions encountered in the buoyancy-driven detachment of a wall-bound pendant drop (see below), characterized by a nonuniform distribution of (nonequilibrium) surface tension with peak values at the advancing tip and in the necking region (near the minimum neck radius) that are approximately twice as large as the initial equilibrium value (Lamorgese and Mauri, 2015, 2016).

Similar considerations can be applied to describe diffusiophoresis, i.e., the migration of a drop induced by a concentration gradient. Consider an isothermal system composed of a drop with radius R and concentration ϕ_d, surrounded by a continuous phase with concentration $\phi_c = 1 - \phi_d$, having an imposed

concentration gradient, $\nabla\phi_c$. Since the width of the interface a is constant, while the concentration drop across the interface, $\Delta\phi_c = \phi_d - \phi_c$, is larger on one side of the drop than on the other (see Fig. 3), a surface tension difference will induce a Marangoni force, which, in turn, leads to the motion of the drop. Concomitantly, the system is phase separating, with the concentration of the drop and that of the continuous phase tending to their equilibrium values, $(\phi_d)_{eq}$ and $(\phi_c)_{eq}$, respectively. Assuming that the mean drop velocity $|\mathbf{V}|$ is much larger than the typical growth rate of the drop, dR/dt, as it phase separates, the concentration around the drop can be considered as approximately equal to its unperturbed value, i.e., it varies linearly with position. Therefore, proceeding as in the thermocapillary migration case, from Eq. (23) we have

$$\mathbf{V} = C\frac{\alpha R D}{a}\nabla\phi_c, \tag{25}$$

where we have considered Eqs. (11) and (18), defining $C = d\kappa/d\phi_c$. This result was presented in Vladimirova et al. (1999a), showing that near the critical point $C \approx \Psi - 2$. A similar treatment was also presented by Karpov and Oxtoby (1997).

2.5. The contact angle

Let us consider a liquid drop lying on a plane surface, at equilibrium with the surrounding fluid. The static equilibrium of the drop can be modeled assuming that the surface tensions at the point of coexistence of the three phases (wall-drop, σ_{wd}, wall-fluid, σ_{wf}, and drop-fluid, $\sigma_{df} \equiv \sigma$) balance each other, thus leading to the well-known Young's condition:

$$\cos\theta = -\frac{\Delta\sigma_w}{\sigma}, \tag{26}$$

where $\Delta\sigma_w \equiv \sigma_{wd} - \sigma_{wf}$ indicates the relative affinity of the wall surface with the drop, relative to that with the fluid. In fact, this relation is key to modeling by phase-field methods a number of contact-line problems in emulsions, including (i) the buoyancy-driven detachment of an isolated, wall-bound pendant drop, and (ii) the motion of an isolated droplet down an incline under gravitational

forces, as detailed below. To study these problems using our phase-field model, its governing equations [Eqs. (12)–(14)] have to be integrated in a channel-like geometry so that no-slip and no-mass-flux boundary conditions become relevant for the velocity and concentration fields at the wall:

$$\mathbf{u} = \mathbf{0}, \qquad \hat{\mathbf{n}} \cdot \nabla \tilde{\mu} = 0, \tag{27}$$

where $\hat{\mathbf{n}}$ is the outward normal from the fluid domain. [Note, however, that Qian et al. (2006) argue in favor of a slip-like velocity boundary condition at the contact line based on microscale arguments.] However, since the Cahn-Hilliard equation is a fourth-order equation, one more boundary condition is required at the wall, expressing the value of the contact angle, i.e., the relative affinity of the wall with the two phases at equilibrium. This is taken care of by the Cahn boundary condition, which follows after minimization of the augmented free energy functional (Lamorgese and Mauri, 2015) as

$$\hat{\mathbf{n}} \cdot \nabla \phi = -\frac{2\kappa}{\sigma a} g_s'(\phi), \tag{28}$$

where, following Jacqmin (2000), a cubic expression in powers of ϕ has been employed for modeling the surface free energy g_s (Lamorgese and Mauri, 2015). Since a knowledge of a and $\Delta\sigma_w$ uniquely identifies the augmented free energy functional, it follows that the Cahn boundary condition can be expressed in terms of those mesoscale parameters as

$$\hat{\mathbf{n}} \cdot \nabla \phi = \frac{12\Delta\sigma_w}{\rho R T a^2 (\Delta\phi_{eq})^3} (\phi - \phi_{eq}^{\alpha})(\phi - \phi_{eq}^{\beta}). \tag{29}$$

However, since results of other models and data in the literature at large are normally expressed in terms of standard macroscale quantities such as equilibrium surface tension and contact angle, Eq. (29) can be conveniently rewritten as

$$\hat{\mathbf{n}} \cdot \nabla \phi = -\frac{12\kappa \cos\theta}{a(\Delta\phi_{eq})^3} (\phi - \phi_{eq}^{\alpha})(\phi - \phi_{eq}^{\beta}). \tag{30}$$

This form is arrived at by noting that since the RHS of Eq. (29) involves a factor of $\Delta\sigma_w/\sigma$, this can be handled by means of Young's equation, Eq. (26),

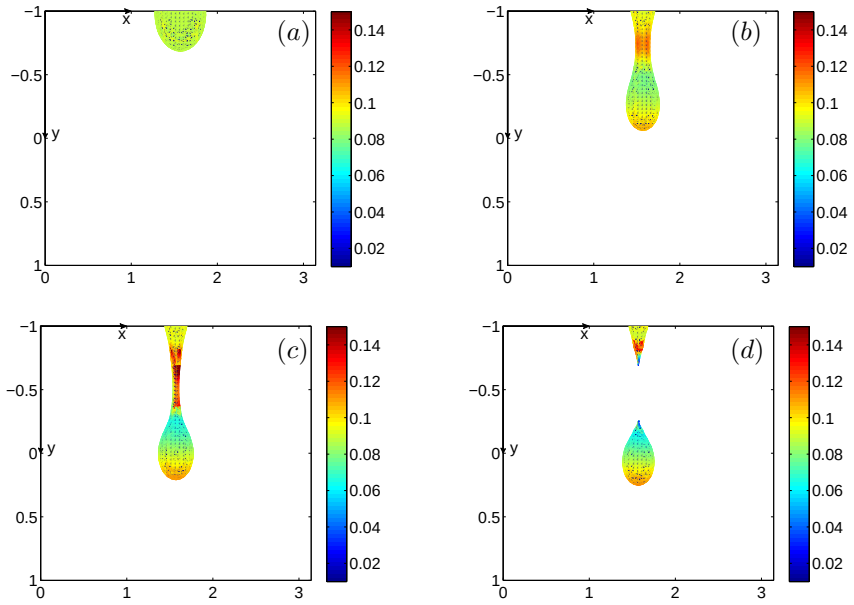

Figure 4: Nonequilibrium surface tension at different nondimensional times (diffusive scaling) $t = 0$, $1.3\,10^{-2}$, $1.55\,10^{-2}$ and $1.6\,10^{-2}$ (left to right and top to bottom) from phase-field simulation with $\theta = 60°$, $Bo/Bo_{cr} \approx 1.53$, and $\Psi = 2.7$, $\alpha = 100$ and $\langle\phi\rangle \approx 0.11$ on a $64 \times 65 \times 64$ grid.

i.e., an additional relation (lying outside of the diffuse-interface framework) that must be invoked to make the connection with the equilibrium contact angle θ. It should be acknowledged that the Cahn boundary condition has been generalized to involve the dynamic contact angle, initially by Jacqmin (2000) and more recently by Carlson et al. (2009) and Yue and Feng (2011). Also, such extensions for binary fluids have been discussed in Sibley et al. (2013c) within a diffuse-interface description of liquid-vapor flows.

At first, 3D simulations of buoyancy-driven detachment were run (Lamorgese and Mauri, 2016) in a computational domain of size $L_x = L_z = \frac{\pi}{2} N \frac{a}{\sqrt{\Psi}}$, $L_y = N \frac{a}{\sqrt{\Psi}}$ ($N = 64$), with a pendant droplet (having a radius of $12a$) of the minority phase deposited on the upper wall with a 90° contact angle (at $t = 0$) and embedded in a continuous phase (with both phases at equilibrium), for calculating critical Bond numbers corresponding to a pinchoff event as a function of static contact angle. We also looked at the nonequilibrium surface tension

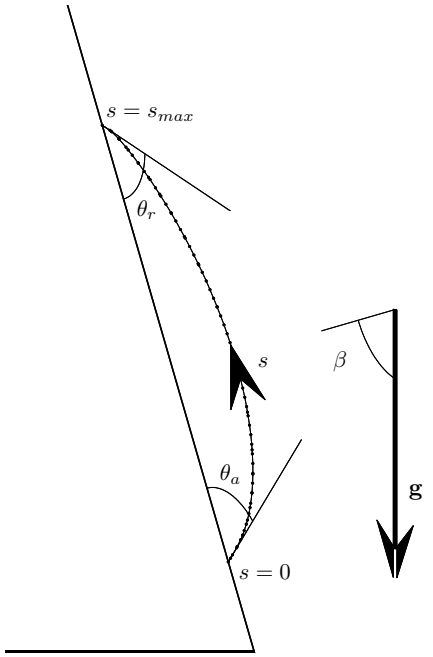

Figure 5: Mass fraction $\tilde{\phi} = 1/2$ isoline at $t = 0.011$ (diffusive time units) from 2D phase-field simulation of drop down an incline with $\beta = 60°$, $\Psi = 2.7$, $\alpha = 100$ and $Bo = 7.1$ with an imposed equilibrium contact angle of 60°. By sending tangents to the droplet profile at its advancing and receding tips, we find $\theta_a \approx 64°$ and $\theta_r \approx 59°$.

[Eq. (2)] in the necking regime of drop detachment, i.e., for $\theta \leq 90°$ and supercritical Bond numbers. Figure 4 shows snapshots of the nonequilibrium surface tension at different (nondimensional) times from a buoyancy-driven detachment simulation with $Bo = 1.53Bo_c$ and $\theta = 60°$. As can be seen, the initial condition (a) corresponds to a uniform distribution of equilibrium surface tension. Subsequently, as the drop shape changes and a neck is formed, the nonequilibrium surface tension becomes nonuniform with peak values of about twice the initial equilibrium value located at the advancing tip and in the necking region near the minimum neck radius. This result is in favor of our previous argument to explain a discrepancy (Lamorgese and Mauri, 2016) between our numerically determined static contact angle dependence of the critical Bond number for detachment of a wall-bound pendant drop and its sharp-interface counterpart based on a static stability analysis after numerical integration of

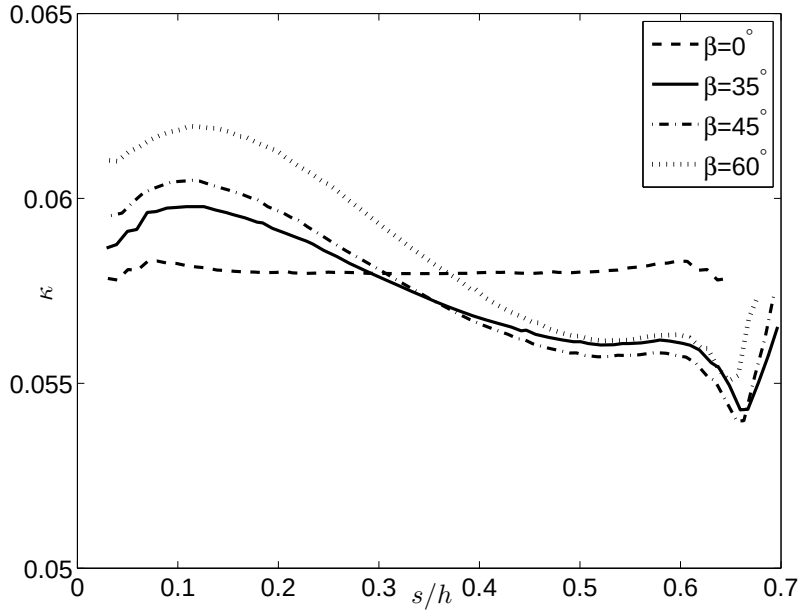

Figure 6: Nonequilibrium surface tension vs. arc length (made dimensionless with the channel half width h) for a droplet profile corresponding to the $\tilde{\phi} = 1/2$ isoline with the drop sliding down an incline having $\beta = 35°$, $45°$, and $60°$ along with $\Psi = 2.7$, $\alpha = 100$, $Bo = 7.1$ (solid, dot-dashed, and dotted) vs. equilibrium surface tension distribution for a droplet with an imposed equilibrium contact angle ($\theta_e = 60°$) in the absence of gravity (dashed). The advancing (resp. receding) tip corresponds to $s = 0$ (resp. $s = s_{max}$).

the Young-Laplace equation. In fact, a sharp-interface analysis together with its assumption of constant surface tension are unable to account for the reduced tendency to detachment due to a sharpening of concentration gradients in the necking region which leads to an effective increase in the nonequilibrium surface tension or an increase in the critical Bond number.

Finally, we comment on our results from phase-field simulations of the motion of an isolated droplet down an incline due to gravitational forces. In our numerical setup, the droplet (having a radius of $7.6a$) is acted upon by the same buoyant force as before (Lamorgese and Mauri, 2015), $\mathbf{F}_g = \rho\mathbf{g}(\phi - \langle\phi\rangle)$, at an angle β with the normal to the incline (see Fig. 5). Again, our mass fraction initial condition corresponds to a quiescent droplet deposited on the incline with a contact angle of 90°. First, we ran a test case to make sure that, in the

β	5°	20°	35°	45°	60°	75°	80°	90°
$\theta_a(0.5)$	60.5°	61.7°	62.7°	63.2°	64°	64.5°	65.5°	65.9°
$\theta_r(0.5)$	59.9°	59.7°	59.2°	59.2°	59.4°	59.5°	59.2°	59.1°

Table 1: Advancing and receding contact angles for a droplet profile corresponding to the $\tilde{\phi} = 0.5$ isoline for different values of tilt angle β and $\Psi = 2.7$, $\alpha = 100$, $Bo = 7.1$, with prescribed equilibrium contact angle $\theta_e = 60°$.

absence of gravity, a drop initially placed on the substrate with a 90° contact angle would relax towards an equilibrium state corresponding to a prescribed contact angle $\theta^* \neq 90°$. We ran this test with $\theta^* = 60°$ and found that starting from 90°, the contact angle decreases monotonically until it reaches a value of about 61° (for times larger than about $30\,a^2/D$) but still decreasing (at a much lower rate) towards 60°. Next, for a prescribed magnitude of the buoyancy force (corresponding to a Bond number of 7.1), we ran 2D simulations with 128×129 grid points at a fixed static contact angle $\theta_e = 60°$ for different values of β. In all cases we found that the drop moves down the incline with a constant speed which increases monotonically with the tilt angle. [Remarkably, in a 2D study of a drop on an inclined (chemically heterogeneous) substrate, Savva and Kalliadasis (2013) also find that the drop can move with a constant velocity.] At each instant in time, droplet profiles were recorded based on the $\tilde{\phi} = 1/2$ isosurface. We also measured the advancing and receding contact angles by sending tangents to the droplet profile at its advancing and receding tips (see Table 1). In all cases where $\theta_e = 60°$ we found a receding contact angle always less than 60°, while the advancing contact angle was found to be an increasing function of β. For example, with $\beta = 60°$ we found $\theta_a \approx 64°$, and $\theta_a \approx 59°$. These results can be explained in terms of the nonequilibrium surface tension. In fact, from Fig. 6 we see that the equilibrium surface tension as a function of arc length is essentially uniform for a droplet on a substrate with $\beta = 0°$; on the other hand, the sliding motion of the drop for $\beta \neq 0°$ gives rise to a nonuniform distribution of nonequilibrium surface tension, attaining a larger (resp. smaller) than equilibrium value at its advancing (resp. receding) tip, and

this, from Young's condition, translates into a larger (resp. smaller) than equilibrium contact angle. Note that our use of Young's equation for determining contact angles under dynamic conditions is consistent with our formulation of the Cahn boundary condition, which had been based on the assumption of a diffusively-controlled local equilibrium at the wall. Finally, we emphasize once more that based on our phase-field formulation which includes a choice of Hermite interpolation for the Cahn boundary condition, under dynamic conditions the advancing and receding contact angles follow as model predictions after specification of a length scale proportional to the equilibrium interface thichness and of the equilibrium contact angle.

3. Conclusions

At variance with previous works suggesting that the surface tension in a phase-field model is fixed, we have discussed a straightforward extension of the surface tension in binary fluid diffuse-interface models to far-from-equilibrium conditions in terms of the integral across an interface profile of the same excess free energy (over its thermodynamic part) as was used for defining the equilibrium surface tension across a flat interface at local equilibrium. Although a similarly defined nonequilibrium surface tension had already been introduced in the past, its significance had been overlooked particularly in diffuse-interface models of emulsion flows far from the critical point. Consequently, we have reviewed some previously published results as they relate to the nonequilibrium surface tension during mixing and demixing processes in regular binary mixtures as well as during Marangoni migration of isolated droplets in a temperature gradient. In particular, at a late stage of the mixing process of an initially phase-separated mixture the nonequilibrium surface tension decays like the inverse square root of time, while in the initial (linear) regime of spinodal decomposition the buildup in the nonequilibrium surface tension is exponential. In addition, we have emphasized that during Marangoni migration of an isolated drop in a temperature or concentration gradient for small values of the Marangoni (and Reynolds) number, the drop goes through a sequence of quasi-

equilibrium states, each one having an (equilibrium) surface tension corresponding to its thermodynamic value. In contrast, far-from-equilibrium conditions are encountered in the buoyancy-driven detachment of a wall-bound pendant drop. In this case, the nonequilibrium surface tension has a nonuniform distribution with peak values that are approximately twice as large as the initial equilibrium value, located at the advancing tip and near the minimum neck radius. Finally, some preliminary results from phase-field simulations of the motion of an isolated droplet down an incline due to gravitational forces have been presented, showing that (i) under dynamic conditions the advancing and receding contact angles follow as model predictions after specification of the equilibrium contact angle and of the characteristic length scale (which represents a coarse-grained equilibrium interface thickness), and that (ii) the hysteresis of dynamic contact angles can be explained in terms of the nonequilibrium surface tension.

Acknowledgements

Financial support provided by MIUR (Grant no. PGR10DN9YV) is gratefully acknowledged.

References

Araki, T., Tanaka, H., 2004. Hydrodynamic delocalization of phase separation in a locally cooled fluid mixture. Europhys. Lett. 65 (2), 214–20.

Archer, A. J., Evans, R., 2004. Dynamical density functional theory and its application to spinodal decomposition. J. Chem. Phys. 121 (9), 4246–54.

Cahn, J. W., 1961. On spinodal decomposition. Acta Metall. 9 (9), 795–801.

Cahn, J. W., Hilliard, J., 1958. Free energy of a nonuniform system. I. Interfacial free energy. J. Chem. Phys. 28, 258–67.

Cahn, J. W., Hilliard, J., 1959. Free energy of a nonuniform system. III. Nucleation in a two-component incompressible fluid. J. Chem. Phys. 31, 688–99.

Califano, F., Mauri, R., 2004. Drop size evolution during the phase separation of liquid mixtures. Ind. Eng. Chem. Res. 43, 349–53.

Califano, F., Mauri, R., Shinnar, R., 2005. Large-scale, unidirectional convection during phase separation of a density-matched liquid mixture. Phys. Fluids 17 (9), 094109.

Carlson, A., Do-Quang, M., Amberg, G., 2009. Modeling of dynamic wetting far from equilibrium. Phys. Fluids 21 (12), 121701.

de Gennes, P.-G., 1985. Wetting: statics and dynamics. Rev. Mod. Phys. 57 (3), 827–63.

de Gennes, P.-G., Brochard-Wyart, F., Quéré, D., 2004. Capillarity and Wetting Phenomena: Drops, Bubbles, Pearls, Waves. Springer.

Goddard, B. D., Nold, A., Kalliadasis, S., 2013. Multi-species dynamical density functional theory. J. Chem. Phys. 138 (14), 144904.

Guo, Z., Lin, P., 2015. A thermodynamically consistent phase-field model for two-phase flows with thermocapillary effects. J. Fluid Mech. 766, 226–71.

Gupta, R., Mauri, R., Shinnar, R., 1999. Phase separation of liquid mixtures in the presence of surfactants. Ind. Eng. Chem. Res. 38, 2418–24.

Henderson, J. R., 1995. Physics beyond van der Waals. Heterog. Chem. Rev. 2 (4), 233–48.

Hohenberg, P. C., Halperin, B. I., 1977. Theory of dynamic critical phenomena. Rev. Mod. Phys. 49, 435–79.

Jacqmin, D., 2000. Contact-line dynamics of a diffuse fluid interface. J. Fluid Mech. 402, 57–88.

Joseph, D. D., Renardy, Y. Y., 1993. Fundamentals of Two-Fluid Dynamics. Part II: Lubricated Transport, Drops and Miscible Liquids. Springer, Chap. X.

Karpov, V. G., Oxtoby, D. W., 1997. Self-organization of growing and decaying particles. Phys. Rev. E 55 (6), 7253–9.

Lamorgese, A., Mauri, R., 2015. Buoyancy-driven detachment of a wall-bound pendant drop: Interface shape at pinchoff and nonequilibrium surface tension. Phys. Rev. E 92, 032401.

Lamorgese, A., Mauri, R., 2016. Critical conditions for the buoyancy-driven detachment of a wall-bound pendant drop. Phys. Fluids 28 (3), 032103.

Lamorgese, A. G., Mauri, R., 2006. Mixing of macroscopically quiescent liquid mixtures. Phys. Fluids 18, 044107.

Lamorgese, A. G., Mauri, R., 2011. Liquid mixture convection during phase separation in a temperature gradient. Phys. Fluids 23, 034102.

Lamorgese, A. G., Molin, D., Mauri, R., 2011. Phase-field approach to multiphase flow modeling. Milan J. Math. 79 (2), 597–642.

Landau, L. D., Lifshitz, E. M., 1980. Statistical Physics, Part I. Pergamon Press, New York, Chaps. 74–76.

Lifshitz, I. M., Slyozov, V. V., 1961. The kinetics of precipitation from supersaturated solid solutions. J. Phys. Chem. Solids 19 (1), 35–50.

Liu, H., Valocchi, A. J., Zhang, Y., Kang, Q., 2013. Phase-field-based lattice Boltzmann finite-difference model for simulating thermocapillary flows. Phys. Rev. E 87 (1), 013010.

Llovell, F., Mac Dowell, N., Blas, F. J., Galindo, A., Jackson, G., 2012. Application of the SAFT-VR density functional theory to the prediction of the interfacial properties of mixtures of relevance to reservoir engineering. Fluid Phase Equilib. 336, 137–50.

Ma, W.-J., Keblinski, P., Maritan, A., Koplik, J., Banavar, J. R., 1993. Dynamical relaxation of the surface tension of miscible phases. Phys. Rev. Lett. 71 (21), 3465–8.

Ma, W.-J., Maritan, A., Banavar, J. R., Koplik, J., 1992. Dynamics of phase separation of binary fluids. Phys. Rev. A 45 (8), R5347–50.

Magaletti, F., Picano, F., Chinappi, M., Marino, L., Casciola, C. M., 2013. The sharp-interface limit of the Cahn-Hilliard/Navier-Stokes model for binary fluids. J. Fluid Mech. 714, 95–126.

Marconi, U. M. B., Tarazona, P., 2000. Dynamic density functional theory of fluids. J. Phys.: Condens. Matter 12 (8A), A413–8.

Mauri, R., Shinnar, R., Triantafyllou, G., 1996. Spinodal decomposition in binary mixtures. Phys. Rev. E 53, 2613–23.

Molin, D., Mauri, R., 2007. Enhanced heat transport during phase separation of liquid binary mixtures. Phys. Fluids 19, 074102.

Onuki, A., 2007. Dynamic van der Waals theory. Phys. Rev. E 75 (3), 036304.

Onuki, A., Kanatani, K., 2005. Droplet motion with phase change in a temperature gradient. Phys. Rev. E 72 (6), 066304.

Osborn, W. R., Orlandini, E., Swift, M. R., Yeomans, J. M., Banavar, J. R., 1995. Lattice Boltzmann study of hydrodynamic spinodal decomposition. Phys. Rev. Lett. 75, 4031–4.

Pismen, L. M., 2001. Non-local diffuse-interface theory of thin films and moving contact line. Phys. Rev. E 64, 021603.

Pismen, L. M., Pomeau, Y., 2000. Disjoining potential and spreading of thin liquid layers in the diffuse-interface model coupled to hydrodynamics. Phys. Rev. E 62 (2), 2480.

Qian, T., Wang, X.-P., Sheng, P., 2006. A variational approach to moving contact line hydrodynamics. J. Fluid Mech. 564, 333–60.

Sagis, L. M., 2011. Dynamic properties of interfaces in soft matter: Experiments and theory. Rev. Mod. Phys. 83 (4), 1367–403.

Sandler, I. S., 2006. Chemical, Biochemical, and Engineering Thermodynamics, 4th Edition. Wiley, New York, Chap. 9.

Santonicola, G., Mauri, R., Shinnar, R., 2001. Phase separation of initially inhomogeneous liquid mixtures. Ind. Eng. Chem. Res. 40 (8), 2004–10.

Savva, N., Kalliadasis, S., 2013. Droplet motion on inclined heterogeneous substrates. J. Fluid Mech. 725, 462–91.

Serrin, J., 1959. Mathematical principles of classical fluid mechanics. In: Encyclopedia of Physics, Vol. VIII/1. Springer, pp. 125–263.

Sibley, D. N., Nold, A., Kalliadasis, S., 2013a. Unifying binary fluid diffuse-interface models in the sharp-interface limit. J. Fluid Mech. 736, 5–43.

Sibley, D. N., Nold, A., Savva, N., Kalliadasis, S., 2013b. The contact line behaviour of solid-liquid-gas diffuse-interface models. Phys. Fluids 25 (9), 092111.

Sibley, D. N., Nold, A., Savva, N., Kalliadasis, S., 2013c. On the moving contact line singularity: Asymptotics of a diffuse-interface model. Eur. Phys. J. E 36 (3), 26.

Swift, M. R., Orlandini, E., Osborn, W. R., Yeomans, J. M., 1996. Lattice Boltzmann simulations of liquid-gas and binary fluid systems. Phys. Rev. E 54 (5), 5041–52.

Tanaka, H., Araki, T., 1998. Spontaneous double phase separation induced by rapid hydrodynamic coarsening in two-dimensional fluid mixtures. Phys. Rev. Lett. 81, 389–92.

van der Waals, J. D., 1894. The thermodynamic theory of capillarity under the hypothesis of a continuous variation of density. Z. Phys. Chem. Stöchiom. Verwandtschaftsl. 13, 657–725, translated and reprinted in J. Stat. Phys. 20, 200–44 (1979).

Vladimirova, N., Malagoli, A., Mauri, R., 1999a. Diffusiophoresis of two-dimensional liquid droplets in a phase-separating system. Phys. Rev. E 60, 2037–44.

Vladimirova, N., Malagoli, A., Mauri, R., 1999b. Two-dimensional model of phase segregation in liquid binary mixtures. Phys. Rev. E 60, 6968–77.

Young, N. O., Goldstein, J. S., Block, M. J., 1959. The motion of bubbles in a vertical temperature gradient. J. Fluid Mech. 6, 350–6.

Yue, P., Feng, J. J., 2011. Wall energy relaxation in the Cahn–Hilliard model for moving contact lines. Phys. Fluids 23 (1), 012106.